

Perturbative Quantum Simulation

Jinzhao Sun^{1,2,3}, Suguru Endo⁴, Huiping Lin^{1,5}, Patrick Hayden⁶, Vlatko Vedral^{2,7}, and Xiao Yuan^{1,5,6,*}

¹*Center on Frontiers of Computing Studies, Peking University, Beijing 100871, China*

²*Clarendon Laboratory, University of Oxford, Parks Road, Oxford OX1 3PU, United Kingdom*


³*Quantum Advantage Research, Beijing 100080, China*

⁴*NTT Computer & Data Science Laboratories, NTT corporation, Musashino, Tokyo 180-8585, Japan*

⁵*School of Computer Science, Peking University, Beijing 100871, China*

⁶*Stanford Institute for Theoretical Physics, Stanford University, Stanford, California 94305, USA*

⁷*Centre for Quantum Technologies, National University of Singapore, Singapore 117543, Singapore*

 (Received 17 November 2021; revised 27 January 2022; accepted 17 August 2022; published 15 September 2022)

Approximation based on perturbation theory is the foundation for most of the quantitative predictions of quantum mechanics, whether in quantum many-body physics, chemistry, quantum field theory, or other domains. Quantum computing provides an alternative to the perturbation paradigm, yet state-of-the-art quantum processors with tens of noisy qubits are of limited practical utility. Here, we introduce perturbative quantum simulation, which combines the complementary strengths of the two approaches, enabling the solution of large practical quantum problems using limited noisy intermediate-scale quantum hardware. The use of a quantum processor eliminates the need to identify a solvable unperturbed Hamiltonian, while the introduction of perturbative coupling permits the quantum processor to simulate systems larger than the available number of physical qubits. We present an explicit perturbative expansion that mimics the Dyson series expansion and involves only local unitary operations, and show its optimality over other expansions under certain conditions. We numerically benchmark the method for interacting bosons, fermions, and quantum spins in different topologies, and study different physical phenomena, such as information propagation, charge-spin separation, and magnetism, on systems of up to 48 qubits only using an $8 + 1$ qubit quantum hardware. We demonstrate our scheme on the IBM quantum cloud, verifying its noise robustness and illustrating its potential for benchmarking large quantum processors with smaller ones.

DOI: [10.1103/PhysRevLett.129.120505](https://doi.org/10.1103/PhysRevLett.129.120505)

A universal quantum computer can naturally simulate the real-time dynamics of any closed finite dimensional quantum system [1], a challenging task for classical computers. While there has been tremendous progress in quantum computing hardware development, including the landmark quantum supremacy and advantage experiments with superconducting and optical systems [2–5], state-of-the-art quantum hardware can still only control tens of noisy qubits [2,5–7]. That is insufficient for the implementation of fault-tolerant universal quantum computing, which requires 10^3 or more physical qubits per logical qubit to suppress the physical error [8]. It is more pragmatic in the near term to focus on the noisy intermediate-scale quantum (NISQ) regime and utilize hybrid methods, which run a shallow circuit without implementing full error correction [9]. Nevertheless, most quantum simulation algorithms, whether targeting NISQ or universal quantum computers, generally entail a number of physical or logical qubits no smaller than the problem size [10–12]. Given that large-scale fault-tolerant quantum computers do not yet exist and there will be significant size constraints even on NISQ devices for the foreseeable future, a pressing question is how to solve large practical problems with limited quantum devices [13,14].

One possibility is to leverage the classical methods that have been developed to solve quantum many-body problems, wherein the most successful one is perturbation theory. This method divides the Hamiltonian into a major but easily solved component and a weak but potentially complicated counterpart, in which case the full dynamics can be expressed as a series expansion [15–20]. However, the ability to solve the major component and compute the higher-order expansions limits the use of perturbation theory in classical simulation of general many-body problems.

Here, we propose perturbative quantum simulation (PQS), which directly simulates the major component on a quantum computer while perturbatively approximates the weak interaction component. Since there is no assumption on the size or interaction of the major component, PQS potentially goes beyond the conventional perturbative approach, and it could simulate classically challenging systems, such as large systems with weak intersubsystem interactions or intermediate systems with general interactions. Compared to universal quantum computing, PQS has limited power for arbitrary problems; yet, the perturbative treatment of the weak component greatly reduces

quantum resources compared with conventional quantum simulation. Notably, PQS runs a shallower circuit with fewer qubits, making it more noise robust and thus useful in benchmarking large quantum devices with smaller ones. Our simulations on the IBM quantum devices demonstrate a significant improvement of the simulation accuracy over direct simulation.

For eigenstate problems, there are considerable hybrid schemes that combine different classical methods, such as density matrix embedding theory [21–24], dynamical mean field theory [25–27], density functional theory embedding [28], quantum defect embedding theory [29,30], tensor networks [31–33], entanglement forging [34,35], virtual orbital approximation [36], quantum Monte Carlo [37–42], etc. Our Letter instead focuses on the different but meaningful dynamics problem, which is based on perturbation theory and fundamentally from the existing ones with different assumptions, limitations, or applications [43].

Background.—We consider to simulate the dynamics of a quantum many-body system. Suppose the whole system is divided into L subsystems according to topological structures or degrees of freedom, like the clustered molecules [55], the Hamiltonian is $H = H^{\text{loc}} + V^{\text{int}}$, where $H^{\text{loc}} = \sum_l H_l$ is the local strong interaction with each H_l acting on the l th subsystem, and $V^{\text{int}} = \sum_j \lambda_j V_j^{\text{int}}$ is the weak perturbative interaction between the subsystems. Here V_j^{int} are different types of interactions with real amplitudes λ_j .

To simulate the dynamics of $U(t) = e^{-iHt}$, a representative perturbation treatment is via Dyson series expansion as

$$U(t) = 1 - i \int_{t_0}^t dt_1 e^{iH^{\text{loc}}(t_1-t_0)} V^{\text{int}} e^{-iH^{\text{loc}}(t_1-t_0)} + \dots \quad (1)$$

Then $U(t)$ becomes a linear combination of trajectories consisting of different sequential unitary operators. When the local Hamiltonians $\{H_l\}$ are solvable, one can further represent the expansion graphically, such as via Feynman diagrams, and compute expectation values of the time evolved state with different graphs corresponding to different expansion terms. A limitation of perturbation theory is the assumption of the simple hence solvable local Hamiltonians, which fails when $\{H_l\}$ become strongly correlated, as that happens in realistic systems. Indeed, even if no interaction under certain partitioning strategy with $V^{\text{int}} = 0$, no classical methods exist that can efficiently simulate the dynamics of general Hamiltonian $H^{\text{loc}} = \sum_l H_l$; otherwise, the computational class of bounded-error quantum polynomial time collapses. In the following, we introduce the framework of PQS, based on which we propose an explicit algorithm mimicking Dyson series expansion and show its optimality over more general theories.

Framework.—Here, we focus on general ways that realize the joint time evolution channel $\mathcal{U}(\rho, T) = U(T)\rho U^\dagger(T)$ by

applying only local operations on each subsystem separately. To do so, we first introduce the concept of local generalized quantum operations

$$\Phi(\rho) = \text{Tr}_E[\mathbf{U}(\rho \otimes |\mathbf{0}\rangle\langle\mathbf{0}|_E)\mathbf{V}^\dagger]. \quad (2)$$

Here we denote ancillary states $|\mathbf{0}\rangle\langle\mathbf{0}|_E = |0\rangle\langle 0|_{E_1} \otimes \dots \otimes |0\rangle\langle 0|_{E_L}$ and unitary operators $\mathbf{U} = U_{1E_1} \otimes \dots \otimes U_{LE_L}$ and $\mathbf{V} = V_{1E_1} \otimes \dots \otimes V_{LE_L}$, where U_{jE_j} and V_{jE_j} represent the operators acting only on the subsystem j and the j th ancilla. While the operation $\Phi(\rho)$ is nonphysical in general, it can be realized effectively using local operations and postprocessing (see Ref. [44]). Note that $\Phi(\rho)$ reduces to local quantum channels when $\mathbf{U} = \mathbf{V}$. The key idea of PQS theories is to decompose the joint evolution into a set of generalized quantum operations, which separately act on each subsystem. By choosing a spanning set of $\{\Phi_k\}$ properly, an infinitesimal evolution governed by the interaction $\mathcal{V}(\delta t)[\rho] = V^{\text{int}}(\delta t)\rho V^{\text{int}}(\delta t)^\dagger$ can be decomposed as

$$\mathcal{V}(\delta t)[\rho] = \mathcal{I}(\rho) + \delta t \sum_k \alpha_k \Phi_k(\rho), \quad (3)$$

where $V^{\text{int}}(\delta t) = e^{-iV^{\text{int}}\delta t}$ represents the interacting unitary operations within duration δt , and \mathcal{I} is the identity operation.

Next, we consider a Trotterized joint evolution as $\mathcal{U}(T) = [\mathcal{V}(\delta t) \circ \mathcal{U}_l(\delta t)]^{T/\delta t}$. Using the decomposition in

Eq. (3), we can then expand $\mathcal{U}(T)$ as a series of different trajectories. Here, each trajectory is defined by which operations act at each time, including the local time evolution $\mathcal{U}_l(\delta t)$ of each subsystem and one of the generalized quantum operation $\Phi_k(\rho)$ that on average emulates the nonlocal effect of \mathcal{V}^{int} . The whole evolution $\mathcal{U}(T)$ is now decomposed as a linear combination of local operations that act separately on each subsystem, which can be effectively realized in parallel. The expectation value of an arbitrary state can be obtained from local measurement results (see Sec. IB in the Supplemental Material [44] for the derivation and implementation).

The above discretized scheme assumes a small discrete timestep and requires us to apply the operations at each time step δt , which is unnecessary since the effect of the weak interacting operation $\mathcal{V}(\delta t)$ in a short time is close to the identity. We address this problem by stochastically applying the operation Φ_k depending on the amplitude of its associated coefficient $|\alpha_k|$. Taking a short time limit $\delta t \rightarrow 0$, we generate each trajectory according to the decomposition in Eq. (3) and stochastically realize the joint time evolution with operations separately acting on each subsystem. The average of different trajectories reproduces the joint dynamics under $\mathcal{U}(T)$. Note that the number of generalized quantum operations required to realize the joint evolution scales proportionally to the interaction strength as $\mathcal{O}(\sum_k |\alpha_k| T)$, and on average the stochastic implementation

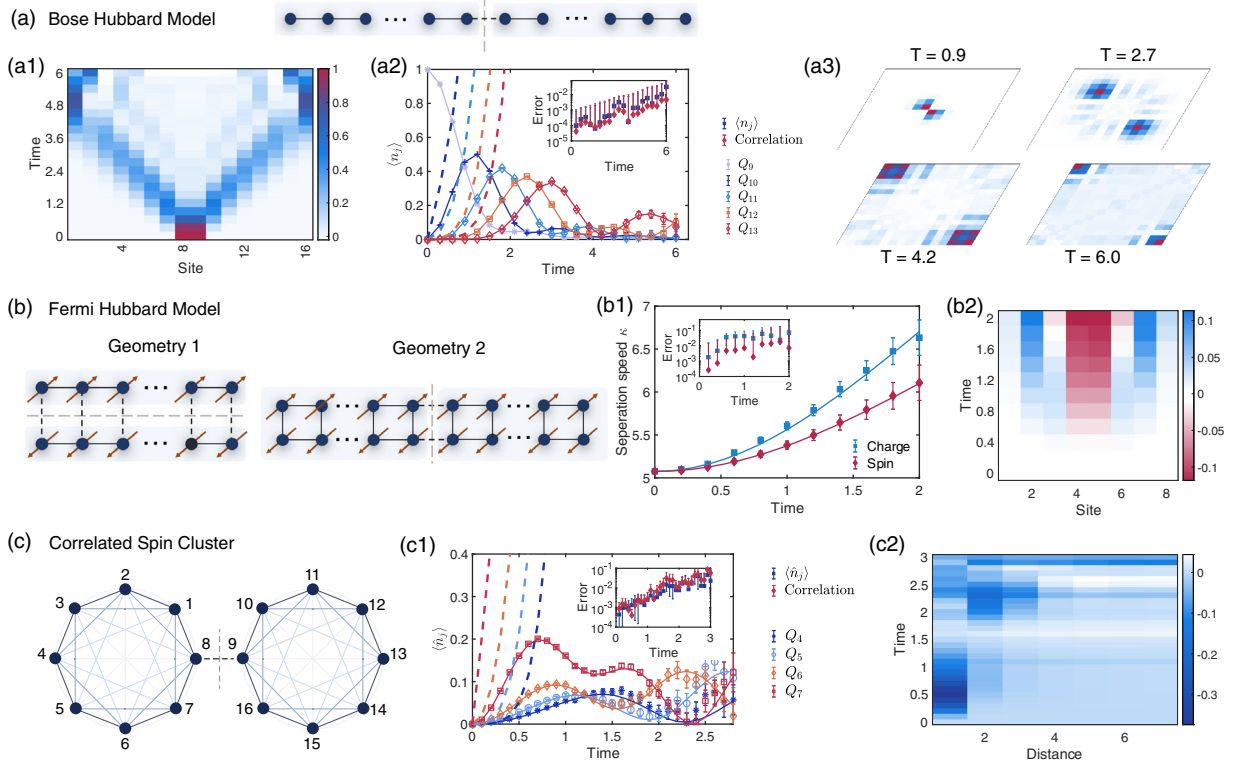


FIG. 1. Dynamics simulation of interacting (a) bosons, (b) fermions, and (c) quantum spin systems with different topologies. Gray dashed lines in site-edge diagrams manifest subsystem partitioning for PQS. We group 8 qubits as a subsystem to simulate $N = 16$ -qubit quantum systems using most 5×10^5 samples. Solid lines represent exact results from direct simulation. (a) Quantum walk (QW) of spinless bosons on a 1D array in the large on site repulsion limit (see Sec. VI in [44] for the Hamiltonian [64]). Two identical bosons are initially excited at the center. (a1) Density spreading $\langle \hat{n}_j \rangle = \langle \hat{b}_j^\dagger \hat{b}_j \rangle$ with bosonic operators \hat{b} under time evolution. (a2) The density distribution at site 9—13 (labeling from left to right). The nearest-neighbor Lieb-Robinson bounds (dashed) capture the density spreading [6,65,66]. The inset shows the errors for the average density and the average density-density correlator $\hat{\rho}_{ij} = \langle \hat{b}_i^\dagger \hat{b}_j^\dagger \hat{b}_i \hat{b}_j \rangle$ with respect to the exact results. (a3) Boson spatial antibunching in QW. The normalized correlator $\hat{\rho}_{ij}/\hat{\rho}_{ij}^{\max}$ at different t [67,68]. (b) Separation of charge and spin density (CSD) in a 1D Fermi-Hubbard model $H = -J \sum_{j,\sigma} (\hat{c}_{j,\sigma}^\dagger \hat{c}_{j+1,\sigma} + \text{H.c.}) + U \sum_j \hat{n}_{j,\uparrow} \hat{n}_{j,\downarrow} + \sum_{j,\sigma} h_{j,\sigma} \hat{n}_{j,\sigma} (\hat{c}_{j,\sigma}, \hat{c}_{j,\sigma}^\dagger$: fermionic operators with spin σ , $U = J = 0.5$) [68]. Left: two partitioning strategies for small and large on-site potential U . The initial state is the ground state of a noninteracting Hamiltonian with quarter filling ($N_\uparrow = N_\downarrow = 2$), in which the CSD are generated in the middle of the chain at $t = 0$ [69–71]. (b1) The separation of charge (blue square) and spin (red diamond) densities. We characterize the separation speed from the middle as $\kappa_\pm = \sum_{j=1}^N |j - (N+1)/2| \langle (\hat{n}_{j,\uparrow} \pm \hat{n}_{j,\downarrow}) \rangle$ for charge (+) and spin (–) degrees of freedom with $\langle \hat{n}_j \rangle = \langle \hat{c}_j^\dagger \hat{c}_j \rangle$ ($N = 8$). The inset shows the errors under evolution. (b2) The difference of CSD under evolution. The relative separation is initially set as 0. (c) Information propagation of correlated Ising spin clusters with power law decay interactions $H_l^{\text{loc}} = \sum_{ij} J_{ij} \hat{\sigma}_{i,i}^x \hat{\sigma}_{i,j}^x + h \sum_j \hat{\sigma}_{i,j}^z$ ($J_{ij} = |i - j|^{-1}$) in the subsystems and interaction $V^{\text{int}} = \hat{\sigma}_{1,N}^x \hat{\sigma}_{2,1}^x$ on the boundary. The initial state is prepared as $|\psi_0\rangle = \hat{\sigma}_8^x |0\rangle^{\otimes N}$. (c1) The signal of quasiparticle excitations at different sites, where the propagation is faster than the nearest-neighbor Lieb-Robinson velocity (dashed) [65,72,73]. (c2) The dynamics of the correlation function $C_d = \langle \hat{\sigma}_8^z \hat{\sigma}_{8+d}^z \rangle - \langle \hat{\sigma}_8^z \rangle \langle \hat{\sigma}_{8+d}^z \rangle$. The inset shows the errors for the averaged quasiparticle excitations’ density and correlation functions.

scheme is proven to be equivalent to the discretized scheme (See Sec. IC in [44]).

By applying our algorithm, the whole simulation process is now decomposed into the average of different ones, each of which only involves operations on the subsystems. Thus, we can effectively simulate nL qubits with operations on subsystems with only $\mathcal{O}(n)$ qubits, and this also offers noise robustness of our method (see Sec. VII in [44]). Note that local dynamics $\mathcal{U}_l(t)$ could be implemented with any

Hamiltonian simulation methods, such as product formulae [57,58] or quantum signal processing [59,60], and our algorithm is compatible with both near-term and fault-tolerant quantum computers.

Explicit protocol.—While the decomposition of Eq. (3) holds in general for an (over)complete set of $\{\Phi_k\}$, it may involve difficult-to-implement operations in experiments. Here, we address this problem by developing an explicit decomposition with only local unitary operations.

Specifically, we consider a natural expansion of $\mathcal{V}(\delta t)$ as

$$\mathcal{V}(\delta t)[\rho] = \mathcal{I}(\rho) - i\delta t \sum_j \lambda_j (V_j^{\text{int}} \rho - \rho V_j^{\text{int}}), \quad (4)$$

where all V_j^{int} are tensor products of unitaries, and hence each term $\mathcal{I}(\rho)$, $V_j^{\text{int}}\rho$, or ρV_j^{int} corresponds to a specific generalized quantum operation. We emphasize that the expansion only involves unitary operations, and avoids the computational cost in diagrammatic perturbation theory, which greatly simplifies the implementation. We further prove (in Theorem 3 in the Supplemental Material [44]) that the explicit decomposition corresponds to the infinite-order Dyson series expansion [61].

Implementing the interaction \mathcal{V} perturbatively using generalized quantum operations introduces a sampling overhead C . Specifically, when measuring the output state of the perturbatively simulated state, the measurement accuracy is $\varepsilon = \mathcal{O}(C\sigma/\sqrt{N_s})$, given N_s samples in contrast to $\varepsilon = \mathcal{O}(1/\sqrt{N_s})$ in direct simulation. Here, σ is the standard deviation introduced from the expansion, normally less than 1. Assuming the general decomposition of Eq. (3), the overhead is $C = e^{\sum_k |\alpha_k| T}$. Different decomposition of Eq. (3) would lead to different coefficients and hence different overhead. We further prove that the explicit decomposition in Eq. (4) has the minimal simulation cost, provided that the Pauli operators of each V_i satisfy a certain mild condition (see Theorem 2 in [44] for the proof of optimality, and an illustrative example in [62]). Since the overhead increases exponentially with $\lambda_T = \sum_i |\lambda_i| T$, PQS cannot simulate arbitrary systems with strong V^{int} or long time T [63]. Yet, the overhead is independent of the initial state, size, and interaction strengths of the subsystems. With a constant λ_T , PQS could be applied to study intricate quantum many-body systems with strong subsystem interactions. As shown shortly, PQS can be used to probe interesting physical phenomena directly, benchmark NISQ processors, simulate large quantum circuits, etc.

Numerical and IBM Cloud results.—We apply PQS to study many-body physical phenomena in different systems with different topological structures. As shown in Fig. 1, we investigate (a) the quantum walk of bosons on a one-dimensional lattice, (b) the separation of charge and spin excitations of fermions with two-dimensional topology, and (c) the correlation propagation of quantum spin systems of two clusters. We design appropriate partitioning strategies, in which the whole system consists of two subsystems and each subsystem consists of 8 qubits. In each example, we present the corresponding task-specific partitioning strategy of the quantum systems. Using the explicit decomposition strategy, we exploit $8 + 1$ qubits to simulate each subsystem and classically emulate the quantum system with numerical results shown in Fig. 1. All unique features

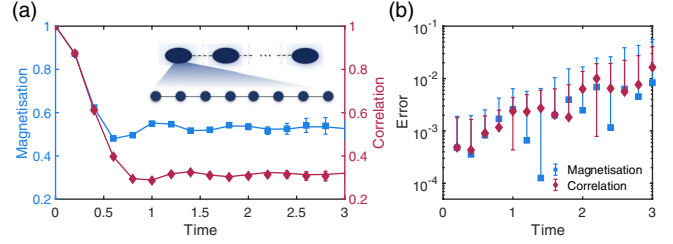


FIG. 2. Dynamics simulation of 1D 48-site spin chains. The subsystem and interaction Hamiltonians are $H_l^{\text{loc}} = \sum_i \hat{\sigma}_{i,i}^x \hat{\sigma}_{i+1,i}^x + \sum_i \hat{\sigma}_{i,i}^z$ and $V_l^{\text{int}} = f_l \hat{\sigma}_{i,N}^x \hat{\sigma}_{i+1,1}^x$, respectively, and the interactions on the boundary are randomly generated from $[0, J/2]$. (a) The average magnetization (in blue) $(1/N) \sum_i \langle \hat{\sigma}_i^z \rangle$ and nearest-neighbor correlation function (in red) $[1/(N-1)] \sum_i \langle \hat{\sigma}_i^z \hat{\sigma}_{i+1}^z \rangle$, compared with the TEBD method as a benchmark. The inset illustrates the geometry of the spin systems and the partitioning strategy where we group 8 adjacent qubits as subsystems. (b) The errors for the average magnetization and correlation using 5×10^5 samples.

are detected just as we directly simulate the whole system. Indeed, the numerical results align with those of the exact simulation, thus verifying the reliability of the theory. We refer to Sec. VI in [44] for other physical systems, including the long-range spin chains, and simulation details.

These numerical tests are restricted to 16 qubits since the exact simulation of larger quantum systems becomes exponentially costly. To benchmark PQS for larger systems, we investigated a 1D 48-site spin chain with nearest-neighbor correlations, using the time-evolving block decimation (TEBD) method with matrix product states as the reference. As shown in Fig. 2, our simulation results coincide with those of TEBD, which again verifies the reliability of PQS for simulating multiple subsystems. Intriguingly, PQS only needs to manipulate $8 + 1$ qubits to recover the joint dynamics of the 48-qubit system.

We only consider the time evolution of small and classically simulable quantum systems for benchmarking our method. However, for all the examples considered here, since the simulation cost is independent of the interaction and initial states of the subsystems, PQS also works when tackling a much larger subsystem with more complicated subsystem interactions. In practice, when we increase the subsystem size to around $n = 50$ qubits and consider general strong interactions, PQS could outstrip the capabilities of classical simulation and reliably probe properties of quantum systems with a small-size quantum processor.

In contrast to direct simulation, PQS could also be more robust to noise attributed to the reduction of quantum sources [74]. To verify such an advantage, we experimentally study the dynamical phase transition of an 8-qubit Ising model with nearest-neighbor correlations on IBMQ hardware. By dividing the system into two subsystems, we use a $4 + 1$ -qubit processor to implement our PQS algorithm and compare the results with conventional direct

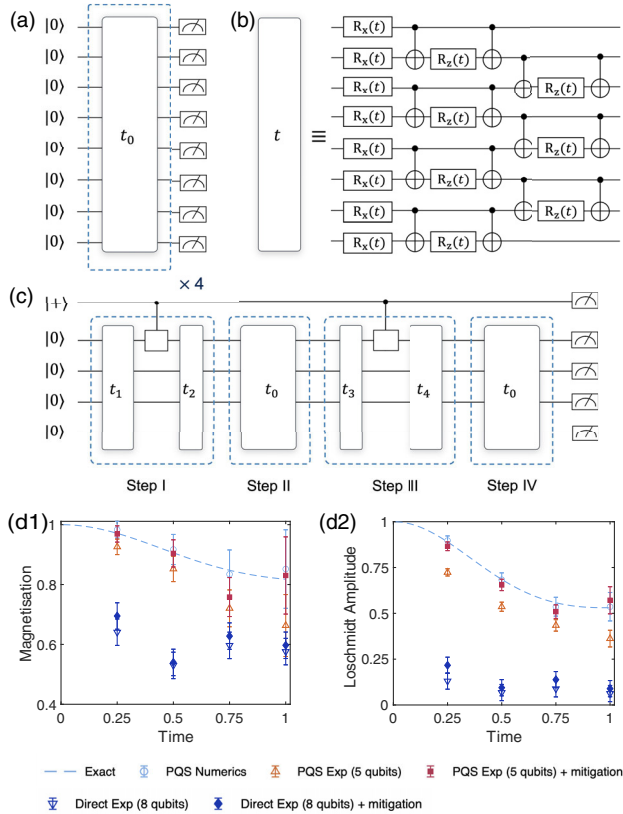


FIG. 3. Implementation and results of the dynamical phase transition of 8 interacting spins. The initial state $|\psi_0\rangle = |0\rangle^{\otimes 8}$ is evolved under an 8-site Ising Hamiltonian $H = \sum_j \delta_j^z \delta_{j+1}^z + 0.5 \sum_j \delta_j^x$ with $T = 1$. (a) Quantum circuit for 8-qubit simulation based on first-order Trotterization with four steps $t_0 = 1/4$. (b) The circuit block for a single-step evolution for time t with parallelization. (c) An example for the implementation of PQS to simulate an 8-qubit system with operations on the 4 + 1 qubit. The circuit blocks are similar as that in (b) with 4 qubits. When a generalized operation is inserted into a Trotter step, we divide the step into two evolutions and insert the operation between that. (d) The magnetization and Loschmidt amplitude in ferromagnetic and paramagnetic phases. Here, the Loschmidt amplitude $\mathcal{G}(t) = |\langle \psi_0 | e^{-iHt} | \psi_0 \rangle|^2$ characterizes the dynamical echo back to the initial state [76], as an indicator of dynamical phase transition when it decreases to 0. We compare the results of exact simulation (dashed line), PQS (numerics, circle), PQS using IBMQ [5 qubits in (c), upper triangle], and the direct simulation using IBMQ [8 qubits in (a), lower triangle]. We also show the results using measurement error mitigation for PQS (solid square) and direct simulation (solid diamond).

simulation with 8 qubits, as shown in Fig. 3. For a total evolution time $T = 1$, a first-order Trotterization is used, which has four steps and a negligible Trotter error. Figures 3(d1) and 3(d2) show the magnetization and Loschmidt amplitude in ferromagnetic phases. The results clearly demonstrate that PQS achieves higher simulation accuracy than direct simulation. It is also found that with measurement error mitigation, PQS approaches the exact

result [75], and outperforms direct simulation consistently. More results and detailed discussions on the implementation and noise robustness of PQS can be found in Sec. VII in [44].

Conclusion and discussion.—Our theoretical, numerical, and simulation results indicate that quantum simulation and perturbation theory are not only compatible but complementary. The PQS algorithm leverages quantum computers to simulate the major component of the Hamiltonian, alleviating the constraint of a classical perturbation method, and uses classical perturbation to approximate the interaction, circumventing limited quantum resources in near-term or early-stage fault-tolerant quantum computers. Since PQS is a hybrid method that combines quantum computing and classical perturbation theory, it inherits their advantages as well as their limitations, such as high-dimensional systems with strong correlations V^{int} and long time T . Yet, PQS is applicable to intermediate-size systems, such as a square lattice with tens to hundreds of qubits, and it is particularly useful for large systems with weak intersubsystem interactions, such as (quasi) one-dimensional systems and clustered subsystems. Our results demonstrate wide applicability of PQS methods for studying new physical phenomena, and its potential application in benchmarking large quantum processors with small ones, an emerging demand in the NISQ era. Meanwhile, we could integrate other classical perturbation treatments of the interaction with quantum computing, such as the one that expands according to the interaction strength. We might also consider other hybrid approaches, such as tensor networks, to effectively solve complex many-body systems while alleviating the simulation cost. One may also apply the idea of PQS to more efficiently emulate large quantum circuits using smaller ones [32,77–81].

J. S. thanks Xiao-Ming Zhang and Chenbing Wang for the valuable discussions. X. Y. was supported by the Simons Foundation and the National Natural Science Foundation of China, Grant No. 12175003. P. H. was supported by AFOSR FA9550-19-1-0369. S. E. is supported by Moonshot R&D, JST, Grant No. JPMJMS2061; MEXT Q-LEAP Grant No. JPMXS0120319794, and PRESTO, JST, Grant No. JPMJPR2114. We acknowledge use of the IBM quantum cloud experience for this work. The views expressed are those of the authors and do not reflect the official policy or position of IBM or the IBMQ team. The numerics are supported by the University of Oxford Advanced Research Computing (ARC) facility and the high-performance Computing Platform of Peking University.

* xiaoyuan@pku.edu.cn

- [1] I. M. Georgescu, S. Ashhab, and F. Nori, *Rev. Mod. Phys.* **86**, 153 (2014).
- [2] F. Arute, K. Arya, R. Babbush, D. Bacon, J. C. Bardin, R. Barends, R. Biswas, S. Boixo, F. G. Brandao, D. A. Buell *et al.*, *Nature (London)* **574**, 505 (2019).

- [3] H.-S. Zhong *et al.*, *Science* **370**, 1460 (2020).
- [4] H.-S. Zhong *et al.*, *Phys. Rev. Lett.* **127**, 180502 (2021).
- [5] Y. Wu *et al.*, *Phys. Rev. Lett.* **127**, 180501 (2021).
- [6] M. Gong, S. Wang, C. Zha, M.-C. Chen, H.-L. Huang, Y. Wu, Q. Zhu, Y. Zhao, S. Li, S. Guo *et al.*, *Science* **372**, 948 (2021).
- [7] X. Mi *et al.*, *Science* **374**, 1479 (2021).
- [8] E. T. Campbell, B. M. Terhal, and C. Vuillot, *Nature (London)* **549**, 172 (2017).
- [9] J. Preskill, *Quantum* **2**, 79 (2018).
- [10] S. McArdle, S. Endo, A. Aspuru-Guzik, S. C. Benjamin, and X. Yuan, *Rev. Mod. Phys.* **92**, 015003 (2020).
- [11] M. Cerezo, A. Arrasmith, R. Babbush, S. C. Benjamin, S. Endo, K. Fujii, J. R. McClean, K. Mitarai, X. Yuan, L. Cincio, and P. J. Coles, *Nat. Rev. Phys.* **3**, 625 (2021).
- [12] K. Bharti, A. Cervera-Lierta, T. H. Kyaw, T. Haug, S. Alperin-Lea, A. Anand, M. Degroote, H. Heimonen, J. S. Kottmann, T. Menke *et al.*, *Rev. Mod. Phys.* **94**, 015004 (2022).
- [13] E. Altman *et al.*, *PRX Quantum* **2**, 017003 (2021).
- [14] B. Bauer, S. Bravyi, M. Motta, and G. K.-L. Chan, *Chem. Rev.* **120**, 12685 (2020).
- [15] A. A. Abrikosov, L. P. Gorkov, and I. E. Dzyaloshinski, *Methods of Quantum Field Theory in Statistical Physics* (Dover Publications Inc., New York, 2012).
- [16] E. Fradkin, *Field Theories of Condensed Matter Physics* (Cambridge University Press, Cambridge, England, 2013).
- [17] M. Rigol, T. Bryant, and R. R. P. Singh, *Phys. Rev. E* **75**, 061118 (2007).
- [18] M. Rigol, T. Bryant, and R. R. P. Singh, *Phys. Rev. Lett.* **97**, 187202 (2006).
- [19] S. Wilson, *Comput. Phys. Rep.* **2**, 391 (1985).
- [20] G. Rohringer, H. Hafermann, A. Toschi, A. A. Katanin, A. E. Antipov, M. I. Katsnelson, A. I. Lichtenstein, A. N. Rubtsov, and K. Held, *Rev. Mod. Phys.* **90**, 025003 (2018).
- [21] G. Knizia and Garnet Kin-Lic Chan, *Phys. Rev. Lett.* **109**, 186404 (2012).
- [22] G. Knizia and G. K.-L. Chan, *J. Chem. Theory Comput.* **9**, 1428 (2013).
- [23] S. Wouters, C. A. Jiménez-Hoyos, Q. Sun, and G. K.-L. Chan, *J. Chem. Theory Comput.* **12**, 2706 (2016).
- [24] N. C. Rubin, [arXiv:1610.06910](https://arxiv.org/abs/1610.06910).
- [25] B. Bauer, D. Wecker, A. J. Millis, M. B. Hastings, and M. Troyer, *Phys. Rev. X* **6**, 031045 (2016).
- [26] I. Rungger, N. Fitzpatrick, H. Chen, C. H. Alderete, H. Apel, A. Cowtan, A. Patterson, D. M. Ramo, Y. Zhu, N. H. Nguyen, E. Grant, S. Chretien, L. Wossnig, N. M. Linke, and R. Duncan, [arXiv:1910.04735](https://arxiv.org/abs/1910.04735).
- [27] H. Chen, M. Nusspickel, J. Tilly, and G. H. Booth, *Phys. Rev. A* **104**, 032405 (2021).
- [28] M. Rossmannek, P. K. Barkoutsos, P. J. Ollitrault, and I. Tavernelli, *J. Chem. Phys.* **154**, 114105 (2021).
- [29] H. Ma, M. Govoni, and G. Galli, *npj Comput. Mater.* **6**, 85 (2020).
- [30] N. Sheng, C. Vorwerk, M. Govoni, and G. Galli, *Nat. Comput. Sci.* **2**, 424 (2022).
- [31] F. Barratt, J. Dborin, M. Bal, V. Stojevic, F. Pollmann, and A. G. Green, *npj Quantum Inf.* **7**, 79 (2021).
- [32] X. Yuan, J. Sun, J. Liu, Q. Zhao, and Y. Zhou, *Phys. Rev. Lett.* **127**, 040501 (2021).
- [33] S. Kanno, S. Endo, Y. Suzuki, and Y. Tokunaga, *Phys. Rev. A* **104**, 042424 (2021).
- [34] A. Eddins, M. Motta, T. P. Gujarati, S. Bravyi, A. Mezzacapo, C. Hadfield, and S. Sheldon, *PRX Quantum* **3**, 010309 (2022).
- [35] P. Huembeli, G. Carleo, and A. Mezzacapo, [arXiv:2205.00933](https://arxiv.org/abs/2205.00933).
- [36] T. Takeshita, N. C. Rubin, Z. Jiang, E. Lee, R. Babbush, and J. R. McClean, *Phys. Rev. X* **10**, 011004 (2020).
- [37] Z.-X. Li and H. Yao, *Annu. Rev. Condens. Matter Phys.* **10**, 337 (2019).
- [38] W. J. Huggins, B. A. O’Gorman, N. C. Rubin, D. R. Reichman, R. Babbush, and J. Lee, *Nature (London)* **603**, 416 (2022).
- [39] X. Xu and Y. Li, [arXiv:2205.14903](https://arxiv.org/abs/2205.14903).
- [40] G. Mazzola and G. Carleo, [arXiv:2205.09203](https://arxiv.org/abs/2205.09203).
- [41] T. L. Patti, O. Shehab, K. Najafi, and S. F. Yelin, [arXiv:2112.02190](https://arxiv.org/abs/2112.02190).
- [42] Y. Zhang, Y. Huang, J. Sun, D. Lv, and X. Yuan, [arXiv:2206.10431](https://arxiv.org/abs/2206.10431).
- [43] The assumptions of the embedding methods and comparisons to our method are discussed in [44].
- [44] See Supplemental Material at <http://link.aps.org/supplemental/10.1103/PhysRevLett.129.120505> for the framework of generalized quantum operations and perturbative quantum simulation, implementation, resource analysis, derivations and proof, higher-order moment analysis, applications and numerical simulations, and demonstrations on IBM quantum devices, which includes Refs. [45–54].
- [45] D. Greenbaum, [arXiv:1509.02921](https://arxiv.org/abs/1509.02921).
- [46] G. Aleksandrowicz, T. Alexander, P. Barkoutsos, L. Bello, Y. Ben-Haim *et al.*, Qiskit: An open-source framework for quantum computing (2019), [10.5281/zenodo.2562111](https://arxiv.org/abs/10.5281/zenodo.2562111).
- [47] S. Endo, S. C. Benjamin, and Y. Li, *Phys. Rev. X* **8**, 031027 (2018).
- [48] J. Sun, X. Yuan, T. Tsunoda, V. Vedral, S. C. Benjamin, and S. Endo, *Phys. Rev. Applied* **15**, 034026 (2021).
- [49] M. Kieferová, A. Scherer, and D. W. Berry, *Phys. Rev. A* **99**, 042314 (2019).
- [50] Y.-H. Chen, A. Kalev, and I. Hen, *PRX Quantum* **2**, 030342 (2021).
- [51] I. H. Kim, [arXiv:1702.02093](https://arxiv.org/abs/1702.02093).
- [52] J. Šmakov, A. L. Chernyshev, and S. R. White, *Phys. Rev. Lett.* **98**, 266401 (2007).
- [53] K. Xu, Z.-H. Sun, W. Liu, Y.-R. Zhang, H. Li, H. Dong, W. Ren, P. Zhang, F. Nori, D. Zheng *et al.*, *Sci. Adv.* **6**, eaba4935 (2020).
- [54] J. Zhang, G. Pagano, P. W. Hess, A. Kyprianidis, P. Becker, H. Kaplan, A. V. Gorshkov, Z.-X. Gong, and C. Monroe, *Nature (London)* **551**, 601 (2017).
- [55] For instance, the lattice Hamiltonian with multiple degrees of freedom and molecular systems with virtual and active orbitals or in a clustered structure (see Refs. [14,17,56] and Sec. V of the Supplemental Material [44] for more discussions) provide a natural partitioning strategy for the subsystems, similarly to that in perturbation theory.

- [56] E. Garlatti, T. Guidi, S. Ansbro, P. Santini, G. Amoretti, J. Ollivier, H. Mutka, G. Timco, I. Vitorica-Yrezabal, G. Whitehead *et al.*, *Nat. Commun.* **8**, 14543 (2017).
- [57] A. M. Childs, D. Maslov, Y. Nam, N. J. Ross, and Y. Su, *Proc. Natl. Acad. Sci. U.S.A.* **115**, 9456 (2018).
- [58] A. M. Childs, Y. Su, M. C. Tran, N. Wiebe, and S. Zhu, *Phys. Rev. X* **11**, 011020 (2021).
- [59] G. H. Low and I. L. Chuang, *Quantum* **3**, 163 (2019).
- [60] G. H. Low and I. L. Chuang, *Phys. Rev. Lett.* **118**, 010501 (2017).
- [61] We discuss the implementation with a truncated expansion on a quantum computer in Sec. III in [44].
- [62] For example, the condition holds when $V^{\text{int}} = \lambda_1 X_a Y_b Z_c + \lambda_2 Y_a Z_b X_c + \lambda_3 Z_a X_b Y_c$ with Pauli operators X , Y , and Z acting on three subsystems a , b , and c . To have a reasonable overhead C , the algorithm is efficient when $\lambda_T = \sum_i |\lambda_i| T = \mathcal{O}(1)$, aligning with the spirit of perturbation theory.
- [63] The sampling cost could be alleviated by implementing finite-order Dyson series expansion. Note that there is a trade-off between the sampling cost and the simulation error.
- [64] Note that the Hamiltonian considered here breaks the translational invariance.
- [65] S. Bravyi, M. B. Hastings, and F. Verstraete, *Phys. Rev. Lett.* **97**, 050401 (2006).
- [66] Z. Yan, Y.-R. Zhang, M. Gong, Y. Wu, Y. Zheng, S. Li, C. Wang, F. Liang, J. Lin, Y. Xu *et al.*, *Science* **364**, 753 (2019).
- [67] Y. Lahini, M. Verbin, S. D. Huber, Y. Bromberg, R. Pugatch, and Y. Silberberg, *Phys. Rev. A* **86**, 011603 (R) (2012).
- [68] M. A. Cazalilla, R. Citro, T. Giamarchi, E. Orignac, and M. Rigol, *Rev. Mod. Phys.* **83**, 1405 (2011).
- [69] F. Arute, K. Arya, R. Babbush, D. Bacon, J. C. Bardin, R. Barends, A. Bengtsson, S. Boixo, M. Broughton, B. B. Buckley *et al.*, [arXiv:2010.07965](https://arxiv.org/abs/2010.07965).
- [70] I. D. Kivlichan, J. McClean, N. Wiebe, C. Gidney, A. Aspuru-Guzik, Garnet Kin-Lic Chan, and R. Babbush, *Phys. Rev. Lett.* **120**, 110501 (2018).
- [71] Z. Jiang, K. J. Sung, K. Kechedzhi, V. N. Smelyanskiy, and S. Boixo, *Phys. Rev. Applied* **9**, 044036 (2018).
- [72] P. Jurcevic, B. P. Lanyon, P. Hauke, C. Hempel, P. Zoller, R. Blatt, and C. F. Roos, *Nature (London)* **511**, 202 (2014).
- [73] C. Monroe, W. C. Campbell, L.-M. Duan, Z.-X. Gong, A. V. Gorshkov, P. W. Hess, R. Islam, K. Kim, N. M. Linke, G. Pagano, P. Richerme, C. Senko, and N. Y. Yao, *Rev. Mod. Phys.* **93**, 025001 (2021).
- [74] A smaller quantum device is usually much more accurate than a larger quantum processor due to crosstalks or other types of errors when controlling large quantum systems. Our method could thus serve as a benchmark of the computing result for large-scale problems.
- [75] S. Bravyi, S. Sheldon, A. Kandala, D. C. McKay, and J. M. Gambetta, *Phys. Rev. A* **103**, 042605 (2021).
- [76] P. Jurcevic, H. Shen, P. Hauke, C. Maier, T. Brydges, C. Hempel, B. P. Lanyon, M. Heyl, R. Blatt, and C. F. Roos, *Phys. Rev. Lett.* **119**, 080501 (2017).
- [77] T. Peng, A. W. Harrow, M. Ozols, and X. Wu, *Phys. Rev. Lett.* **125**, 150504 (2020).
- [78] F. Barratt, J. Dborin, M. Bal, V. Stojevic, F. Pollmann, and A. G. Green, *npj Quantum Inf.* **7**, 79 (2021).
- [79] K. Mitarai and K. Fujii, *New J. Phys.* **23**, 023021 (2021).
- [80] K. Fujii, K. Mitarai, W. Mizukami, and Y. O. Nakagawa, [arXiv:2007.10917](https://arxiv.org/abs/2007.10917).
- [81] K. Mitarai and K. Fujii, *Quantum* **5**, 388 (2021).